Quantum efficiency roll-off at high brightness in fluorescent and phosphorescent organic light emitting diodes

N. C. Giebink[1,2] and S. R. Forrest[2,*]

[1]*Department of Electrical Engineering, Princeton University, Princeton, New Jersey 08544, USA*

[2]*Departments of Electrical Engineering and Computer Science, and Physics, University of Michigan, Ann Arbor, Michigan 48109, USA*

(Received 30 March 2008; published 23 June 2008)

A general technique is demonstrated to quantify the contribution of monomolecular and bimolecular quenching processes to the external quantum efficiency (EQE) roll-off in organic light emitting devices (OLEDs). Based on the photoluminescence transients of electrically driven devices, we identify the relative contributions of quenching and lack of charge balance to the roll-off in four fluorescent and phosphorescent devices containing the dopants 2,3,7,8,12,13,17,18-octaethylporphine platinum (PtOEP), *fac* tris-2-phenylpyridine iridium [$Ir(ppy)_3$], the laser dye 4-dicyanmethylene-2-methyl-6-(*p*-dimethylaminostyryl)-4*H*-pyran (DCM), and neat tris(8-hydroxyquinoline) aluminum. We find that quenching is proportional to the radiative lifetime of the emitting molecule and that it is solely responsible for the roll-off of PtOEP. Roll-off of the EQE for $Ir(ppy)_3$ is due primarily to loss of charge balance at low current density, J, and only shows significant quenching at $J \geq 1$ A/cm^2. No quenching is observed for the fluorescent doped DCM device, even for $J \sim 28$ A/cm^2. Consequently, doped fluorescent OLEDs that maintain charge balance at high current density enable the elimination of intensity roll-off, which may provide a route to electrically pumped organic lasing.

DOI: 10.1103/PhysRevB.77.235215 PACS number(s): 73.50.Gr, 73.61.Ph, 78.55.Kz

I. INTRODUCTION

Organic light emitting devices (OLEDs) have matured as a technology for use in both large-area displays[1,2] and solid-state lighting.[3] Such devices commonly exhibit low operating voltages,[4] 100% internal quantum efficiencies,[5] and long operational lifetimes.[6] In most OLEDs, however, both the external quantum and power efficiencies decrease[7–10] monotonically with increasing current density (and brightness) after peaking in the range of 0.1–10 mA/cm^2. Efficient operation at high brightness is needed for displays to offset the finite pixel aperture ratio, and it is especially important for passive-matrix configurations,[11] where the required brightness scales with the number of rows in the display. Efficiency targets for OLEDs in white lighting applications are also typically specified[12] at high brightness (>850 cd/m^2). Finally, the prospect of demonstrating an electrically pumped organic laser diode has been shown[13] to depend on the product of current density and external quantum efficiency (EQE).

The sources of EQE roll-off at high intensities are twofold: imbalance between the numbers of electrons and holes in the emissive layer (EML) and nonradiative exciton quenching processes. Joule heating can also play a role, but it is effectively managed[14] with pulsed operation and increased substrate thermal conductivity, and so will not be considered here. The majority of attention to date has focused on the role of quenching processes as the source of roll-off, with triplet-triplet exciton annihilation[9,15,16] often proposed for phosphorescent devices, and singlet-singlet,[14,17] singlet polaron,[18–20] and field induced[21–24] quenching for fluorescent devices.

Using the photoluminescence (PL) transient of an electrically driven OLED, we demonstrate a general method to quantify the contributions of exciton quenching and charge imbalance to quantum efficiency roll-off. This technique is applied to both fluorescent and phosphorescent OLEDs having emissive dopant natural decay lifetimes spanning the range from 2.7 ns to 56.3 μs. Four devices using different emitters are studied. These include tris(8-hydroxyquinoline) aluminum (Alq_3), Alq_3 doped with 4-dicyanmethylene-2-methyl-6-(*p*-dimethylaminostyryl)-4*H*-pyran (DCM) laser dye,[25] *fac* tris-2-phenylpyridine iridium [$Ir(ppy)_3$], and 2,3,7,8,12,13,17,18-octaethylporphine platinum (PtOEP) doped into the host 4,4′-bis(9-carbazolyl)-2,2′-biphenyl (CBP).[8,26] We find that exciton quenching dominates the roll-off for the device with the longest dopant lifetime (PtOEP) but that its contribution decreases as the lifetime is reduced. For the shortest lifetime material combination (DCM:Alq_3), no quenching is observed, and loss of charge balance accounts entirely for the EQE roll-off at high brightness.

This paper begins with a description of the measurement concept and theory in Sec. II. Device preparation and experimental methods are described in Sec. III, and in Sec. IV, data are presented, with relative loss pathways quantified. Section V analyzes the roll-off of each device and demonstrates reduced roll-off for a device with improved charge balance. Conclusions are presented in Sec. VI.

II. THEORY

The electrically pumped PL transient method, which has been previously used in unipolar devices,[19] provides a means to quantify the quenching rate of emissive excitons as a function of drive current. Conceptually, a small, optically excited population of excitons is exposed to all of the quenching processes present in the emissive layer of an OLED. Monitoring the transient decay of this population as a function of current density allows the quenching rate to be quantified.

The total light emitting exciton density, $N(x,t)$, in the EML of an OLED is

$$N(x,t) = N_{EL}(x) + N_{PL}(x,t), \tag{1}$$

where $N_{EL}(x)$ is the electrically generated emitting exciton distribution in steady state and $N_{PL}(x,t)$ is a small perturbation due to an absorbed optical pulse. In a fluorescent device, $N(x,t)$ represents dopant singlet excitons, and in a phosphorescent device, it represents triplets. Under optical excitation, Förster transfer from the host efficiently populates the dopant singlet state,[25] followed by rapid intersystem crossing to the triplet state in the case of a phosphor.[27] The time dependence of $N(x,t)$ is as follows:

$$\frac{d}{dt}[N(x,t)] = G(x,J) - N(x,t)\left[\frac{1}{\tau} + K_{agg}(x,J)\right], \tag{2}$$

where $G(x,J)$ is the electrical generation rate of $N_{EL}(x)$ at current density J, τ is the natural exciton lifetime, and $K_{agg}(x,J)$ is an aggregate rate due to quenching by all monomolecular and bimolecular processes.[10] Now, $K_{agg}(x,J)$ can be expressed as

$$K_{agg}(x,J) = [\gamma_n n(x) + \gamma_p p(x) + \gamma_{NN} N_{EL}(x) + \zeta(F) + \cdots], \tag{3}$$

which includes bimolecular reactions such as exciton-polaron $[\gamma_n n(x)$ and $\gamma_p p(x)]$ and exciton-exciton $[\gamma_{NN} N_{EL}(x)]$ annihilations, as well as quenching, $\zeta(F)$, due to the local electric field, F.[10,28]

Substituting Eq. (1) into Eq. (2) and separating the steady-state and transient portions, we obtain

$$N_{EL}(x) = \frac{G(x,J)}{[1/\tau + K_{agg}(x,J)]}, \tag{4a}$$

$$\frac{dN_{PL}(x,t)}{dt} = -N_{PL}[1/\tau + K_{agg}(x,J)]. \tag{4b}$$

Diffusion for the population $N_{EL}(x)$ is implicit in Eq. (4a) through the generation profile $G(x,J)$. In Eq. (4b), it is neglected because the intensity of the exciting optical pulse varies gradually across the thin emissive layer, so $\partial^2 N_{PL}(x,t)/\partial x^2$ is small.

Since both the steady-state electroluminescence (EL) intensity, I_{EL}, and transient photoluminescence intensity, $I_{PL}(t)$, are proportional to $N_{EL}(x)$ and $N_{PL}(x,t)$, respectively, we have

$$I_{EL} = C \int \frac{G(x,J)}{[1/\tau + K_{agg}(x,J)]} dx, \tag{5a}$$

$$I_{PL}(t) = C \exp(-t/\tau) \int N_{PL}(x,0) \exp[-K_{agg}(x,J)t] dx, \tag{5b}$$

where C is a constant accounting for radiative rate, outcoupling, and geometric factors. From continuity, the generation rate is related to the local electron (J_n) and hole (J_p) current densities via

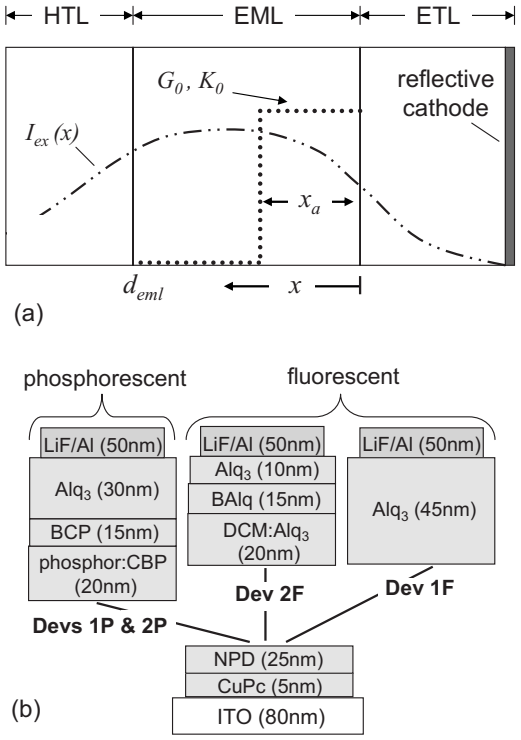

FIG. 1. (a) Schematic diagram of the device model, showing a step approximation to the recombination zone (dotted line) of width x_a, and the PL excitation profile, $I_{ex}(x)$, generated by the N_2 laser pulse. The emissive exciton generation rate in the recombination zone is G_0, and the quenching rate is K_0. (b) Device structures of the four OLEDs studied.

$$G(x,J) = \frac{1}{q}\frac{d[J_n(x)]}{dx} = -\frac{1}{q}\frac{d[J_p(x)]}{dx}. \tag{6}$$

The total generation rate in the EML is thus

$$\int G(x,J)dx = \frac{1}{q}[J_{Cn} - J_{An}] = \frac{1}{q}[J_{Ap} - J_{Cp}] \to \frac{1}{q}Jb, \tag{7}$$

where $J_{An}(J_{Ap})$ and $J_{Cn}(J_{Cp})$ are the electron and hole current densities at the anode and cathode sides of the emissive layer, respectively. Thus,

$$b = \frac{[J_{Ap} - J_{Cp}]}{J} = \frac{[J_{Cn} - J_{An}]}{J} \tag{8}$$

is the charge balance factor,[29] which is the probability that a hole or electron injected into the emissive layer recombines before exiting.

For simplicity, we assume that generation is uniform across the recombination zone[30] of width x_a, as shown in Fig. 1(a). Thus, $G(x,J)=G_0$ at $0<x<x_a$, and $G(x,J)=0$ elsewhere. Since both charge and exciton densities, as well as the electric-field intensity, are all highest in the recombination zone, then $K_{agg}(x,J)$ has a similar functional form. Hence, $K_{agg}(x,J)=K_0$ at $0<x<x_a$, and $K_{agg}(x,J)=0$ elsewhere.

Substituting these expressions into Eq. (5a) and using Eq. (7) yield

$$I_{EL} = C\frac{J}{q}\left[\frac{b}{1/\tau + K_0}\right] \tag{9}$$

for the OLED electroluminescence intensity. Given that the EQE is proportional to I_{EL}/J, we obtain

$$\mathrm{EQE}(J) = \frac{b(J)}{b_{\max}}\left[\frac{1}{1+\tau K_0(J)}\right]\mathrm{EQE}_{\max}, \tag{10}$$

where $\mathrm{EQE}_{\max}$ is the maximum value of EQE as a function of current density. At $\mathrm{EQE}_{\max}$, quenching is assumed to be negligible ($K_0 \sim 0$), and the charge balance factor b is taken at its maximum, $b_{\max}$. Equation (10) shows that a decrease in EQE is due either to a reduction of the charge balance, $b(J)$, or to an increase in the nonradiative quenching rate, $K_0(J)$.

Using Eq. (5b) with the optical excitation profile, $I_{ex}(x)$, and the step approximation for $K_{agg}(x,J)$, as in Fig. 1(a), we obtain biexponential decay for the OLED PL transient as the following:

$$I_{PL}(t) = C'\left\{\exp[-(1/\tau + K_0)t]\int_0^{x_a} I_{ex}(x)dx + \exp[-(t/\tau)]\int_{x_a}^{d_{EML}} I_{ex}(x)dx\right\}. \tag{11}$$

The constants of proportionality between $I_{ex}(x)$ and $N_{PL}(x,0)$ are combined in the constant C'. Here, $I_{ex}(x)$ is calculated by the transfer-matrix method[31] according to the incident angle, polarization, and material layer optical constants for the excitation wavelength. Since τ, $I_{ex}(x)$, and the EML width, d_{EML}, are all known, fits to Eq. (11) yield $K_0(J)$ as well as the evolution of the recombination zone width, x_a, as a function of drive current.

III. EXPERIMENT

All devices were grown on prepatterned, solvent cleaned, indium-tin-oxide (ITO) coated glass.[32] The ITO was UV-ozone treated prior to thermal evaporation of the organic layers in a vacuum system with a base pressure of $\sim 10^{-7}$ Torr. The device structures are shown in Fig. 1(b). The hole injection and transport layer (HTL) is comprised of a 5 nm thick copper phthalocyanine (CuPc) layer followed by a 25 nm thick layer of 4,4′-bis[*N*-(1-naphthyl)-*N*-phenyl-amino]-biphenyl (NPD). The phosphorescent emissive layers are each 20 nm thick and consist of CBP doped with 6 wt % PtOEP in device 1P and 8 wt % $\mathrm{Ir(ppy)_3}$:CBP in device 2P. On top of the phosphorescent EML, a 15 nm thick 2,9-dimethyl-4,7-diphenyl-1,10-phenanthroline (BCP) hole and exciton blocking layer is deposited, followed by a 30 nm thick $\mathrm{Alq_3}$ electron-transport layer.

In the fluorescent device 1F, a 45 nm thick neat $\mathrm{Alq_3}$ layer serves as both EML and electron transporting layer (ETL). No blocking layer was used, making it comparable to a conventional NPD-$\mathrm{Alq_3}$ device. The fluorescent device 2F emissive layer [see Fig. 1(b)] is 20 nm thick, consisting of 3 wt % DCM doped into $\mathrm{Alq_3}$. This is capped with a 15 nm thick aluminum(III)bis(2-methyl-8-quinolinato)4-phenylphenolate (BAlq) hole and exciton blocking layer, followed by a 10 nm thick ETL of $\mathrm{Alq_3}$.

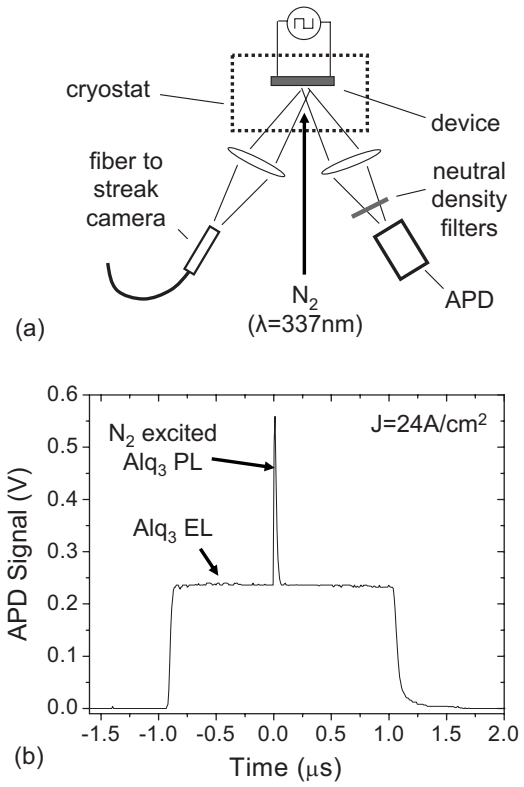

FIG. 2. (a) Schematic of the experimental setup. Emissive layer photoluminescence transients excited by the N_2 laser from the electrically driven device are measured using either a streak camera or an avalanche photodiode (APD). (b) Typical luminescence transient showing both EL and PL of device 1F due to a 2 μs electrical pulse of current density 24 $\mathrm{A/cm^2}$.

All devices were completed by depositing a 0.8 nm thick layer of LiF followed by an 80 nm thick Al cathode to form 1 $\mathrm{mm^2}$ square devices. Immediately following deposition, the current-voltage-luminance (*I-V-L*) characteristic was measured in atmosphere using a calibrated photodiode and an HP4155 parameter analyzer. Multiple sweeps were conducted to ensure that stable *I-V-L* values were obtained. The device was then loaded into an electrically and optically accessible cryostat and subsequently evacuated to 50 mTorr.

Pulsed *I-V-L* measurements were conducted using a HP8114A pulse generator at a repetition rate of 10 Hz, and a pulse duration sufficient to ensure that steady-state operation was achieved. Emission was collected at 30° from normal and focused onto a 150 MHz bandwidth avalanche photodiode (APD) preamp combination, with appropriate neutral density filters to prevent signal saturation. A 200 MHz oscilloscope was used to measure the preamp output, the OLED voltage, and the current.

The PL transients were obtained by focusing the output of a pulsed N_2 laser at normal incidence onto a 1 mm diameter spot (1.3 ± 0.2 $\mu\mathrm{J/cm^2}$ and 0.8 ns pulse width at wavelength $\lambda = 337$ nm) within the device area [see Fig. 2(a)]. The laser pulse was synchronized to arrive in the middle of each electrical pulse. An example is shown in Fig. 2(b) for device 1F,

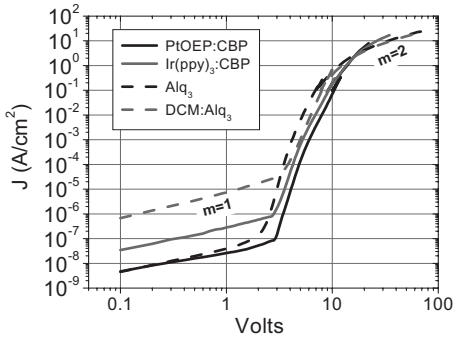

FIG. 3. Current density–voltage characteristics of the four devices studied. All devices show an Ohmic region ($V<2$ V), a high power-law region ($m>2$), and a transition to trap-filled space charge limited current at high bias.

where the APD signal shows the superposition of Alq_3 PL and Alq_3 EL. The phosphorescent device PL decays were obtained with the APD, while a Hamamatsu C4334 streak camera was used to collect the fluorescent transients [see Fig. 2(a)]. For each device, PL transients were taken at $J=0$ A/cm^2 both before and after testing to determine if degradation occurred during the high current measurements.

IV. RESULTS

The current density–voltage (J-V) characteristics for each of the four OLEDs are provided in Fig. 3. Each device shows Ohmic behavior (i.e., $J\sim V$) at low voltage. This is followed by a high power-law region (i.e., $J\sim V^m$, where $m\sim 11$), indicative of interface limited injection[33] from the LiF/Al cathode or to trapped-charge limited transport in the bulk.[32] At high bias, all devices transition to the trap-filled limit and exhibit the characteristic $m=2$ dependence. The functional similarity among the different J-V characteristics reflects the use of the same HTL (CuPc/NPD) and ETL (Alq_3) in each device.

Figure 4 shows the PL transient data as a function of OLED current density for each of the four devices (gray lines), as well as the corresponding fits to Eq. (11) (black lines). In Fig. 4(a), quenching is observed in PtOEP:CBP at increasing J as indicated by the rapid initial decay in the biexponential transient. All curves exhibit the natural PtOEP lifetime, $\tau\sim 56.3$ μs, at long times ($t>80$ μs).

The situation is similar for Ir(ppy)$_3$:CBP in Fig. 4(b), except that the onset of quenching occurs at higher current density (~ 1 A/cm^2), and its magnitude is reduced. This is consistent with the expectation for reduced bimolecular annihilation in Ir(ppy)$_3$ due to its shorter natural lifetime of $\tau=0.63$ μs. The signal spike near $t=0$ of Figs. 4(a) and 4(b) is due to fluorescence excited from the transport layers (NPD, Alq_3); it is readily distinguished from the slow phosphorescence and decays completely within ~ 0.1 μs. For the fluorescent devices, EML fluorescence is spectrally distinguished from that due to the transport layers.

Quenching in device 1F of Fig. 4(c) is only evident at relatively high current density ($J>2$ A/cm^2), where the decay becomes biexponential. The DCM:Alq_3 transients of Fig. 4(d) are monoexponential and show no quenching up to the maximum current density of $J=28$ A/cm^2; however, there is a decrease in amplitude of the $t=0$ luminescence peak. This amplitude decrease is also observed to lesser extents in the other devices and is likely due to exciton dissociation by the high electric field on a picosecond time scale.[28,34–36]

Fits of the data in Fig. 4 to Eq. (11) are provided in Fig. 5. The quenching inferred for PtOEP:CBP is manifest in Fig.

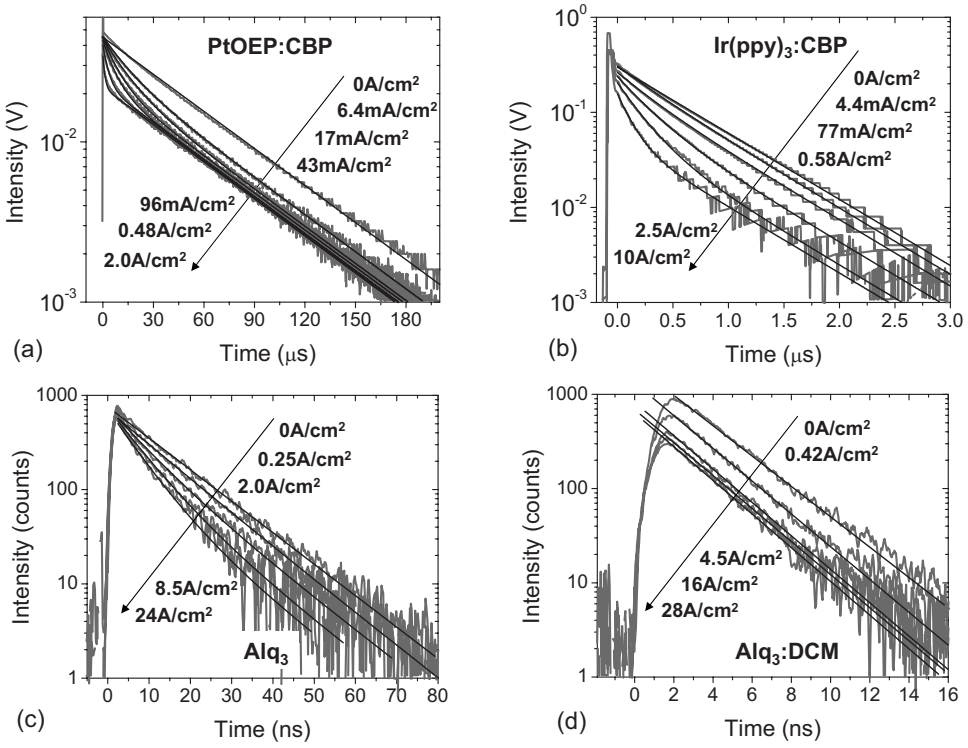

FIG. 4. Photoluminescence transients of the four, electrically driven OLEDs as a function of current density (gray lines) and the fits according to Eq. (11) of the text (black lines). Strong quenching that increases with current density is clear from the biexponential decay of the PtOEP:CBP device in (a). It becomes progressively less pronounced for the cases of Ir(ppy)$_3$:CBP and Alq_3 devices in (b) and (c), respectively. The lifetime of the DCM:Alq_3 device in (d) is monoexponential and constant for all current densities.

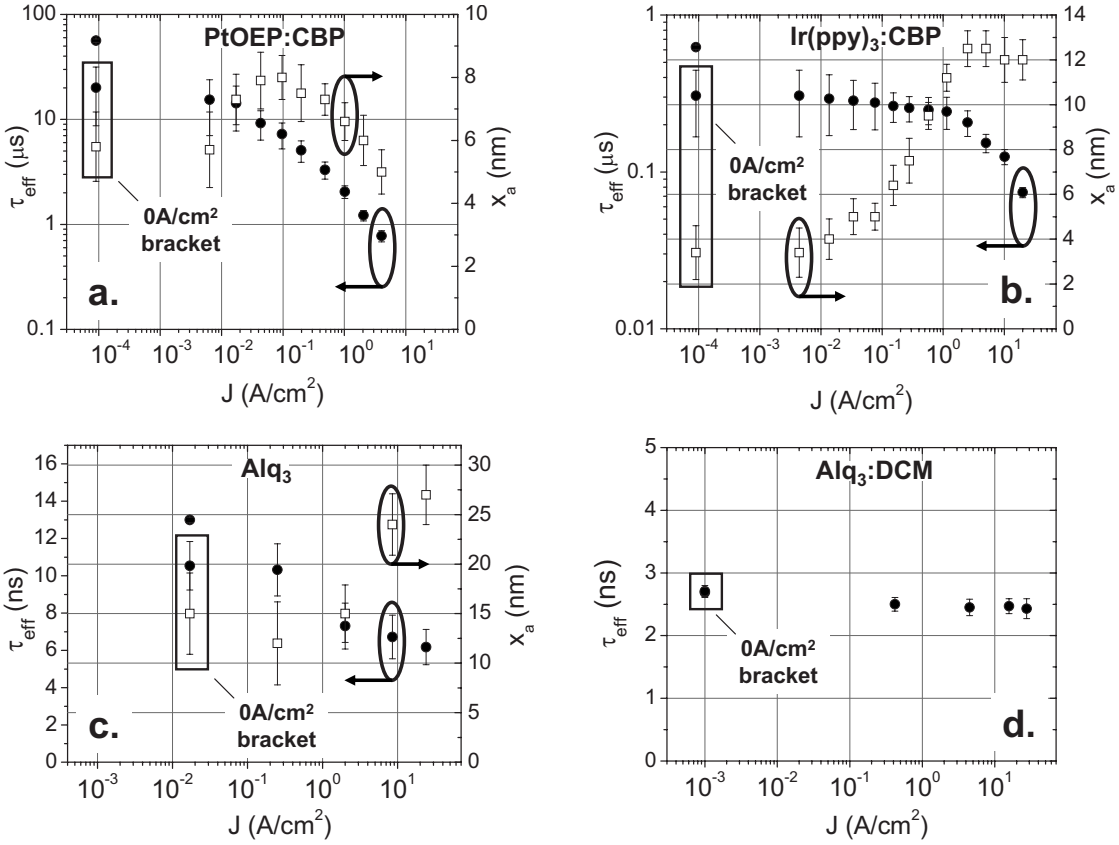

FIG. 5. Fitting results, as a function of current density, for each of the four devices. The quenching rate, K_0, is incorporated into the effective lifetime, $\tau_{eff}=[\tau^{-1}+K_0]^{-1}$, plotted on the left-hand scale, and the recombination zone width, x_a, is plotted on the right-hand scale. Quenching is strongest in the case of PtOEP:CBP and progressively decreases in magnitude for $Ir(ppy)_3$:CBP and Alq_3 devices, disappearing completely for DCM:Alq_3. No recombination width is fit in (d), since the transients of DCM:Alq_3 are monoexponential. The bracketed data points, designated by the large rectangles, are taken at $J=0$ A/cm^2 at the conclusion of electrical pulsing for each device. In (a)–(c), they are different than the $J=0$ A/cm^2 transients taken prior to pulsing and thus indicate that some device degradation occurred over the course of experiment.

5(a), where the effective exciton lifetime in the recombination zone, $\tau_{eff}=[1/\tau+K_0]^{-1}$, decreases by almost 2 orders of magnitude, from 56.3 to ~ 0.8 μs due to the increase in nonradiative decay rate, K_0. The recombination zone width, x_a, is assumed to be adjacent to the EML/ETL interface,[26] as shown in Fig. 1(a). According to Fig. 5(a), x_a initially increases and then decreases as J is increased, indicating possible movement of the recombination zone from one side of the EML to the other. Note that the $J=0$ A/cm^2 data point taken after pulsing indicates some degradation over the course of measurement since the lifetime does not fully recover to the initial value of 56.3 μs.

In Fig. 5(b), $Ir(ppy)_3$:CBP also exhibits quenching at $J>1$ A/cm^2. The recombination zone width of this device is initially $x_a=3$ nm, adjacent to the EML/ETL interface,[37] and increases to $x_a=12$ nm at high J. For the Alq_3 device of Fig. 5(c), only a small amount of quenching is evident, with τ_{eff} decreasing from $\tau=13$ ns to $\tau_{eff}=6$ ns. Here, the recombination zone expands from the HTL/EML interface with increasing current density. Similar to Fig. 5(a), the $J=0$ A/cm^2 PL lifetime taken following the pulsed experiments, for both $Ir(ppy)_3$:CBP and Alq_3 devices, indicates some device degradation during the measurement.

Insignificant quenching is observed for the DCM:Alq_3 device in Fig. 5(d). Here, only an $\sim$7% reduction in effective lifetime is observed at the peak current density of 28 A/cm^2. The transients are monoexponential, which prevents the recombination width, x_a, from being extracted from the fit. Interestingly, no degradation is evident for this device, despite being driven at a higher current density than the others.

Figure 6 shows the EQE roll-off of each device in terms of the quenching and charge balance components of Eq. (10). Measured EQE data are shown as open circles, and solid circles depict the reduction from the measured EQE peak calculated using the fit $K_0(J)$ due only to the quenching term, $[1+\tau K_0(J)]^{-1}$, of Eq. (10). According to Eq. (10), any difference between the data and the quenching term must be due to the reduction in charge balance, $b/b_{\max}$, shown as open triangles.

Quenching accounts for nearly all of the PtOEP:CBP roll-off, as shown in Fig. 6(a). The calculated charge balance is $>90\%$ of its maximum up to a current density $J\sim 2$ A/cm^2. For the $Ir(ppy)_3$:CBP device [Fig. 6(b)], loss of charge balance is significant at low currents, declining to 50% of its maximum by $J=1$ A/cm^2. Quenching also plays a role, however, it only becomes significant when the current

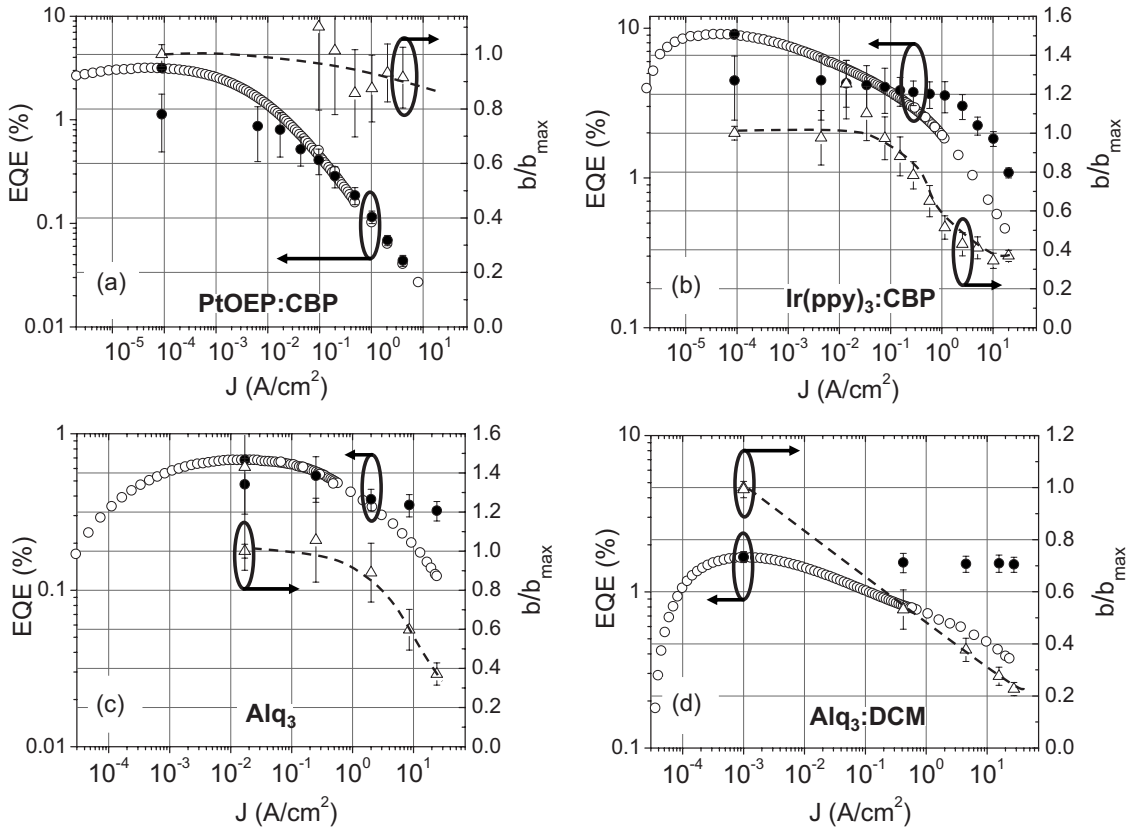

FIG. 6. External quantum efficiency (EQE) roll-off in each of the four devices, showing the contributions of total quenching and loss of charge balance, calculated using Eq. (10) and the fitted data of Fig. 4. EQE data are shown with open circles. The magnitude of the quenching term in Eq. (10) (see text) is plotted using closed circles and represents the reduction of EQE from the measured peak that can be accounted for by quenching. The difference between data and calculated quenching contribution is due to a decrease in charge balance factor, b, shown with open triangles. Quenching accounts for nearly all of the roll-off in the PtOEP:CBP device, while charge balance loss dominates the EQE roll-off of Ir(ppy)$_3$:CBP at low current density, with significant quenching at $J \geqslant 1$ A/cm^2. Loss of charge balance accounts for most of the roll-off in the Alq$_3$ bilayer device, and for all of the roll-off in DCM:Alq$_3$, which shows no quenching contribution.

density exceeds 1 A/cm^2. The Alq$_3$ EQE roll-off of Fig. 6(c) exhibits contributions due to both loss mechanisms. This is in contrast to the DCM:Alq$_3$ device shown in Fig. 6(d), which shows no quenching; the roll-off in this device is due entirely to reduction in charge balance.

Figure 7 shows the EL spectra as a function of current density for the PtOEP:CBP, Ir(ppy)$_3$:CBP, and DCM:Alq$_3$ devices. Spectra at $J > 1$ A/cm^2 were acquired under pulsed drive. In Fig. 7(a), only PtOEP emission, peaking at $\lambda_{pk} = 650$ nm, is observed for current densities up to 0.1 A/cm^2. At 1 A/cm^2, PtOEP singlet emission[38] at $\lambda = 545$ nm is observed in addition to very weak emission from the Alq$_3$ ETL.

The spectra of Fig. 7(b) show pure Ir(ppy)$_3$ emission ($\lambda_{pk} = 515$ nm) at low current density, with a contribution due to emission from the NPD HTL at $\lambda = 450$ nm that appears at $J \geqslant 0.1$ A/cm^2. It is unclear whether there is Alq$_3$ ETL emission at high current densities since it would be dominated by the overlapping Ir(ppy)$_3$ spectrum. Figure 7(c) shows pure DCM emission at $\lambda = 580$ nm at low current density. The high energy shoulder that increases in intensity with J is due to a combination of fluorescence from the BAlq and Alq$_3$ transport layers. Spectra were also measured for the Alq$_3$ undoped EML; only pure Alq$_3$ emission was observed.

To determine the dependence of the EQE roll-off on changes in charge balance, we fabricated the following device with a BAlq blocking layer: ITO which was not UV-ozone treated/NPD (120 nm)/3 wt % DCM:Alq$_3$ (5 nm)/BAlq (10 nm)/1:1 molar ratio Li:Alq$_3$ (30 nm), followed by a LiF/Al cathode as previously described. The EQE of this device is shown in Fig. 8, along with that from the original DCM:Alq$_3$ device 2F, reproduced for comparison. Both devices have comparable peak efficiencies, however, the roll-off of the second device is significantly reduced. From Fig. 8, the roll-off exponent, m, is less than half that of device 2F.

V. DISCUSSION

Previous studies have concluded that the roll-off of PtOEP:CBP devices is due predominantly to triplet-triplet (T-T) annihilation.[16] The results of Fig. 6(a) support this, with nearly all of the roll-off accounted for by quenching. In this case, the quenching rate of Eq. (3) simplifies to $K_{agg}(x,J) \sim \gamma_{T\text{-}T} N_T(x)$.

The roll-off of devices with relatively short lifetime, iridium phosphors such as Ir(ppy)$_3$, cannot be accurately modeled assuming only T-T annihilation. It has been suggested that the combination of both T-T and triplet-polaron (T-P) processes,[9] or field-induced quenching,[23] can fully explain

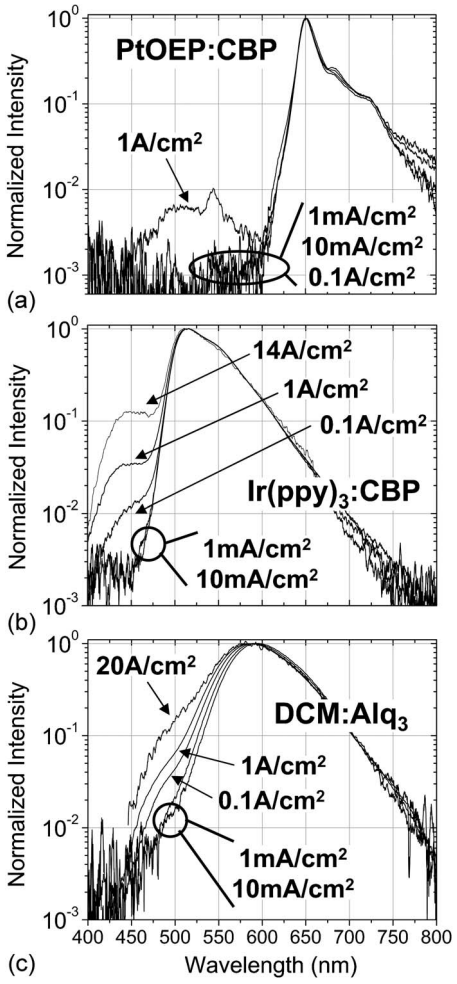

FIG. 7. Electroluminescence spectra as functions of current density for the (a) PtOEP:CBP, (b) $Ir(ppy)_3$:CBP, and (c) DCM:Alq_3 devices. Strong NPD emission in (b) confirms electron leakage into the HTL of the $Ir(ppy)_3$:CBP device, while Alq_3 ETL emission in (c) implies hole leakage out of the DCM:Alq_3 EML to the cathode. Transport layer emission is much weaker in the case of PtOEP:CBP, suggesting that charge balance is maintained at higher current density in this device.

the roll-off of these devices. Here, however, the roll-off is dominated by reduced charge balance at low J, according to Fig. 6(b). Indeed, quenching (which includes both T-T and T-P terms) only becomes significant at $J>1$ A/cm^2. This is in agreement with previous estimations[15,23] of the critical current density at which T-T and T-P quenching becomes significant in doped $Ir(ppy)_3$ OLEDs.

The spectra of Fig. 7(b) qualitatively support the loss of charge balance in the $Ir(ppy)_3$:CBP device, showing NPD transport layer emission at $J \geqslant 0.1$ A/cm^2, which corresponds to the onset of reduced charge balance in Fig. 6(b), due to electron leakage through the HTL. While hole leakage into the ETL may also occur, the resulting Alq_3 emission would be masked by that of $Ir(ppy)_3$. Although significant energy barriers exist to prevent carrier leakage out of the EML, they may be overcome at high fields by processes such as Poole–Frenkel emission[28] or Fowler–Nordheim tunneling,[39] due to charge buildup at such interfaces.[40]

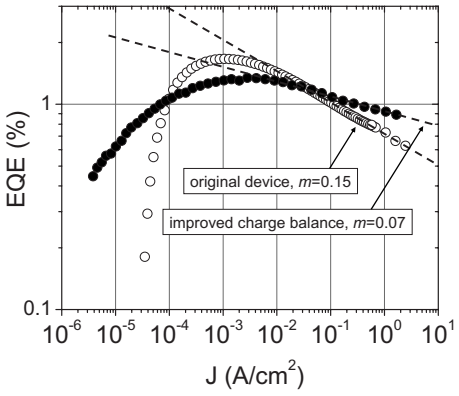

FIG. 8. Reduced EQE roll-off for a DCM:Alq_3 device (closed circles) with improved charge balance, obtained by decreasing hole transport in the HTL and increasing the electron conductivity of the ETL. The EQE data for device 2F (open circles) are reproduced from Fig. 6(d) for comparison.

Since the transport layers are identical for both phosphor devices, it is surprising that charge leakage out of the $Ir(ppy)_3$:CBP EML should be so much greater than for the PtOEP:CBP EML [see Figs. 6(a) and 6(b)]. The spectra of Fig. 7(a) nevertheless support this conclusion, with no evidence of emission from the transport layer at $J \leqslant 0.1$ A/cm^2. At $J=1$ A/cm^2, weak Alq_3 ETL emission appears, indicating leakage of holes to the cathode.

The particular dopant, therefore, significantly influences charge transport and hence the carrier balance in the recombination zone.[41] It has been shown that doping CBP with phosphorescent guests changes both the electron and hole mobilities by several orders of magnitude.[42] Highest occupied molecular-orbital (HOMO) energies of CBP, $Ir(ppy)_3$, and PtOEP have been measured by photoelectron spectroscopy as 6.1, 5.6, and 5.3 eV, respectively.[43,44] The lowest unoccupied molecular-orbital (LUMO) energies for these materials, estimated from the difference between the HOMO level and the optical absorption gap, are, respectively, 2.9, 3.0, and 3.2 eV. Thus, PtOEP forms both a significantly deeper hole and electron trap when doped into CBP compared with those created by $Ir(ppy)_3$. As a result, we speculate that the electron mobility of the PtOEP:CBP EML is significantly lower than that of $Ir(ppy)_3$:CBP, increasing the likelihood of recombination with a hole in the EML prior to escape into the HTL.

According to Fig. 6(c), the roll-off of the Alq_3 fluorescent bilayer device is primarily due to loss of charge balance at low current density, while quenching contributes at $J>2$ A/cm^2. Intensity roll-off in similar devices has previously been modeled assuming only singlet-singlet (S-S) annihilation;[14] however, it has been shown that the bimolecular rate coefficient, $\gamma_{S\text{-}S}$, is too small to account for the EQE roll-off at low current density ($J<10$ A/cm^2).[17] Here, the EL spectra show pure Alq_3 emission for all values of J, hence the carrier leakage must be due to holes that reach the cathode without recombining. Numerical studies of NPD-Alq_3 bilayer devices support this interpretation, showing significant hole leakage to the cathode at low bias.[29,40]

Since no quenching is observed for the DCM:Alq_3 fluorescent device, the efficiency loss is fully accounted for by a

reduction in charge balance, where $b/b_{\max}$ decreases from unity to 0.25 at $J=28$ A/cm^2. Fast field-induced exciton dissociation is evident from the decrease in $t=0$ amplitude of the transients in Fig. 4(d), however, this mode of quenching occurs on a time scale $t \ll \tau$. When the end result is the formation of a stable, dopant exciton, one cannot distinguish whether an exciton forms and then immediately dissociates or whether it never forms at all. Hence, the effect of ultrafast field-induced exciton dissociation is implicit in $b/b_{\max}$, which may reconcile the results of steady-state field-induced PL quenching studies[24,36] with our conclusions here.

The decrease in $b/b_{\max}$ for this device is due to hole leakage to the cathode, as evidenced by the BAlq and Alq_3 emission shoulder that increases with J in the EL spectra shown in Fig. 7(c). Since this device is hole rich, modifications to improve electron transport to the EML and to reduce the total hole current were made, leading to the device with reduced roll-off shown in Fig. 8. Reduced hole injection efficiency (due to the use of ITO untreated by UV-ozone exposure) increased resistance due to a thicker HTL and increased electron current due to use of the high-conductivity Li-doped ETL results in improved charge balance. This supports the conclusion that charge balance is the principle efficiency loss mechanism, since changing only the transport layer characteristics significantly reduces the intensity roll-off for the same EML.

Maintaining perfect charge balance, a DCM:Alq_3 doped fluorescent device should exhibit no roll-off, even at high current density. Indeed, using a combination of doped, highly conductive transport layers and a DCM:Alq_3 EML, even lower roll-off than that of Fig. 8 has been demonstrated.[45] Zero roll-off was recently demonstrated for another fluorescent OLED having doped transport layers[46] and also for an organic light emitting transistor.[47]

Previous work by Khramtchenkov *et al.*[39] has shown that the transition to charge imbalance at high bias follows whenever field dependent injection barriers exist for either carrier at the contacts or within the device. Although energy barriers can prevent charge leakage at low bias, they are readily surmounted in the high-field limit and thus become ineffective. However, from Eq. (8), b becomes fixed when $J_{Ap}=J_{Cn}$, and leakage currents are small. Thus, balanced carrier injection to the EML is more effective in maintaining charge balance than the use of blocking layers. Since the hole and electron currents injected into the EML (J_{Ap} and J_{Cn}) are complicated functions of the energy barriers and transport layer drift and/or diffusion, Ohmic hole and electron injection into the EML is the simplest means to maintain charge balance.

In this limit, the anode (cathode) side of the EML can source infinite hole (electron) current, which ensures that recombination is always complete. Practically, this also requires Ohmic injecting contacts and highly conductive transport layers with no energy barrier into the emissive layer. Indeed, these are the conditions claimed for the zero roll-off OLED.[46]

From Fig. 6, the contribution of quenching to the reduction in EQE decreases with dopant natural lifetime. For PtOEP:CBP where $\tau=56.3$ μs, τ_{eff} decreases by almost 2 orders of magnitude from $J=0$ to $J=4$ A/cm^2, while for DCM:Alq_3 where $\tau=2.7$ ns, there is almost no change in τ_{eff} up to $J=28$ A/cm^2. This is a general trend suggested by Eq. (10), where the magnitude of the quenching is inversely proportional to τ. This is due to the fact that, as τ decreases, excitons have less time to interact with quenching sites and species.

Achieving low or zero roll-off should be possible for many fluorescent doped OLEDs, provided that charge balance is maintained. This has implications for high-brightness OLEDs and for electrically pumped organic semiconductor lasers (OSL). We caution, however, that although no quenching is evident up to $J=28$ A/cm^2, minimum OSL thresholds are predicted[13] to be of order $J_{th} \sim 1$ kA/cm^2, where quenching might prove to be significant.

VI. CONCLUSION

A method based on the measurement of PL transients in electrically driven OLEDs is used to quantify the relative contributions of quenching processes and charge balance loss to quantum efficiency roll-off at high current densities. We apply it to four OLED structures, with dopant lifetimes ranging from 56.3 μs to 2.7 ns. The EQE roll-off of the PtOEP:CBP device is due solely to quenching. In contrast, the Ir(ppy)$_3$:CBP OLED is dominated by loss of charge balance at low current density ($J \leqslant 1$ A/cm^2), showing significant quenching only at high current densities ($J > 1$ A/cm^2). The conventional bilayer Alq_3 OLED efficiency rolls off primarily due to declining charge balance and exhibits quenching at $J > 2$ A/cm^2. The DCM:Alq_3 device shows no quenching for $J \leqslant 28$ A/cm^2, with charge imbalance completely accounting for the observed roll-off. The roll-off behavior of DCM:Alq_3 is shown to be significantly improved by improving carrier balance in the emissive layer.

We show that the quenching component of the EQE decrease is proportional to the natural lifetime of the emissive species. This work implies that the EQE roll-off of phosphorescent OLEDs with short ($\tau \sim 1$ μs) lifetimes can be largely prevented up to $J \simeq 1$ A/cm^2 by improving the characteristics of the charge transport layers. Fluorescent doped OLEDs studied are only limited by quenching at $J > 28$ A/cm^2. If charge balance can be maintained, efficient, ultraintense OLEDs are a possible route to electrically pumped lasing.

ACKNOWLEDGMENTS

The authors thank the Air Force Office of Scientific Research and Universal Display Corp. for partial support of this work.

*stevefor@umich.edu

[1] M. Pfeiffer, S. R. Forrest, K. Leo, and M. E. Thompson, Adv. Mater. (Weinheim, Ger.) **14**, 1633 (2002).

[2] J. J. Brown, V. I. Adamovich, B. Ma, B. D'Andrade, R. C. Kwong, and M. S. Weaver, in *7th International Meeting on Information Display*, Daegu, South Korea, August 27–31, 2007 (unpublished).

[3] B. D'Andrade, Nat. Photonics **1**, 33 (2007).

[4] G. F. He, M. Pfeiffer, K. Leo, M. Hoffmann, J. Birnstock, R. Pudzich, and J. Salbeck, Appl. Phys. Lett. **85**, 3911 (2004).

[5] C. Adachi, M. A. Baldo, M. E. Thompson, and S. R. Forrest, J. Appl. Phys. **90**, 5048 (2001).

[6] M. S. Weaver, R. C. Kwong, V. A. Adamovich, M. Hack, and J. J. Brown, J. Soc. Inf. Disp. **14**, 449 (2006).

[7] C. W. Tang, S. A. Vanslyke, and C. H. Chen, J. Appl. Phys. **65**, 3610 (1989).

[8] M. A. Baldo, S. Lamansky, P. E. Burrows, M. E. Thompson, and S. R. Forrest, Appl. Phys. Lett. **75**, 4 (1999).

[9] S. Reineke, K. Walzer, and K. Leo, Phys. Rev. B **75**, 125328 (2007).

[10] J. Kalinowski, W. Stampor, J. Mezyk, M. Cocchi, D. Virgili, V. Fattori, and P. DiMarco, Phys. Rev. B **66**, 235321 (2002).

[11] K. Mori, Y. Sakaguchi, Y. Iketsu, and J. Suzuki, Displays **22**, 43 (2001).

[12] M. Stolka, *Organic Light Emitting Diodes for General Illumination Update 2002* (Optoelectronics Industry Development Association, Washington D.C., 2002).

[13] M. A. Baldo, R. J. Holmes, and S. R. Forrest, Phys. Rev. B **66**, 035321 (2002).

[14] H. Nakanotani, H. Sasabe, and C. Adachi, Appl. Phys. Lett. **86**, 213506 (2005).

[15] W. Staroske, M. Pfeiffer, K. Leo, and M. Hoffmann, Phys. Rev. Lett. **98**, 197402 (2007).

[16] M. A. Baldo, C. Adachi, and S. R. Forrest, Phys. Rev. B **62**, 10967 (2000).

[17] J. Mezyk, J. Kalinowski, F. Meinardi, and R. Tubino, Chem. Phys. Lett. **395**, 321 (2004).

[18] Y. C. Luo, H. Aziz, G. Xu, and Z. D. Popovic, Chem. Mater. **19**, 2288 (2007).

[19] M. Ichikawa, R. Naitou, T. Koyama, and Y. Taniguchi, Jpn. J. Appl. Phys., Part 2 **40**, L1068 (2001).

[20] R. H. Young, C. W. Tang, and A. P. Marchetti, Appl. Phys. Lett. **80**, 874 (2002).

[21] W. Stampor, J. Kalinowski, P. DiMarco, and V. Fattori, Appl. Phys. Lett. **70**, 1935 (1997).

[22] J. Kalinowski, J. Mezyk, F. Meinardi, R. Tubino, M. Cocchi, and D. Virgili, J. Appl. Phys. **98**, 063532 (2005).

[23] J. Kalinowski, W. Stampor, J. Szmytkowski, D. Virgili, M. Cocchi, V. Fattori, and C. Sabatini, Phys. Rev. B **74**, 085316 (2006).

[24] Y. C. Luo, H. Aziz, Z. D. Popovic, and G. Xu, Appl. Phys. Lett. **89**, 103505 (2006).

[25] V. G. Kozlov, V. Bulovic, P. E. Burrows, M. A. Baldo, V. B. Khalfin, G. Parthasarathy, S. R. Forrest, Y. You, and M. E. Thompson, J. Appl. Phys. **84**, 4096 (1998).

[26] D. F. O'Brien, M. A. Baldo, M. E. Thompson, and S. R. Forrest, Appl. Phys. Lett. **74**, 442 (1999).

[27] Y. Kawamura, K. Goushi, J. Brooks, J. J. Brown, H. Sasabe, and C. Adachi, Appl. Phys. Lett. **86**, 071104 (2005).

[28] M. Pope and C. Swenberg, *Electronic Processes in Organic Crystals and Polymers* (Oxford University Press, New York, 1999).

[29] B. Ruhstaller, S. A. Carter, S. Barth, H. Riel, W. Reiss, and J. C. Scott, J. Appl. Phys. **89**, 4575 (2001).

[30] J. Kalinowski, L. C. Palilis, W. H. Kim, and Z. H. Kafafi, J. Appl. Phys. **94**, 7764 (2003).

[31] L. A. A. Pettersson, L. S. Roman, and O. Inganas, J. Appl. Phys. **86**, 487 (1999).

[32] P. E. Burrows, Z. Shen, V. Bulovic, D. M. McCarty, S. R. Forrest, J. A. Cronin, and M. E. Thompson, J. Appl. Phys. **79**, 7991 (1996).

[33] M. A. Baldo and S. R. Forrest, Phys. Rev. B **64**, 085201 (2001).

[34] R. Kersting, U. Lemmer, M. Deussen, H. J. Bakker, R. F. Mahrt, H. Kurz, V. I. Arkhipov, H. Bassler, and E. O. Gobel, Phys. Rev. Lett. **73**, 1440 (1994).

[35] V. Gulbinas, Y. Zaushitsyn, H. Bassler, A. Yartsev, and V. Sundstrom, Phys. Rev. B **70**, 035215 (2004).

[36] J. Szmytkowski, W. Stampor, J. Kalinowski, and Z. H. Kafafi, Appl. Phys. Lett. **80**, 1465 (2002).

[37] C. Adachi, R. kwong, and S. R. Forrest, Org. Electron. **2**, 37 (2001).

[38] J. Kalinowski, W. Stampor, J. Szmytkowski, M. Cocchi, D. Virgili, V. Fattori, and P. DiMarco, J. Chem. Phys. **122**, 154710 (2005).

[39] D. V. Khramtchenkov, H. Bassler, and V. I. Arkhipov, J. Appl. Phys. **79**, 9283 (1996).

[40] E. Tutis, D. Berner, and L. Zuppiroli, J. Appl. Phys. **93**, 4594 (2003).

[41] J. Kalinowski, L. C. Picciolo, H. Murata, and Z. H. Kafafi, J. Appl. Phys. **89**, 1866 (2001).

[42] M. A. Parshin, J. Ollevier, and M. Van der Auweraer, in *Proceedings SPIE Conference on Organic Optoelectronics And Photonics II*, Strasbourg, France, 2006, Vol. 6192, p. A1922.

[43] I. G. Hill and A. Kahn, J. Appl. Phys. **86**, 4515 (1999).

[44] I. G. Hill, A. J. Makinen, and Z. H. Kafafi, Appl. Phys. Lett. **77**, 2003 (2000).

[45] T. Matsushima and C. Adachi, Appl. Phys. Lett. **89**, 253506 (2006).

[46] T. Matsushima and C. Adachi, Appl. Phys. Lett. **92**, 063306 (2008).

[47] T. Takenobu, Z. Zulkarnaen, T. Takahashi, M. Yahiro, C. Adachi, and Y. Iwasa, Phys. Rev. Lett. **100**, 066601 (2008).